NUMERICAL INVESTIGATION OF HYDROGEN LEAKAGE FROM A HIGH-PRESSURE TANK AND PIPELINE

Nagase, Y.[1], Taira, Y.[2], Sugiyama, Y.[3], Kubota, S.[4], Saburi, T.[5] and Matsuo, A.[6]
[1] Graduate School of Science and Technology, Keio University, 3-14-1 Hiyoshi, Kohoku, Yokohama, Kanagawa 223-8522, Japan, yuri_nagase.28@keio.jp
[2] Graduate School of Science and Technology, Keio University, 3-14-1 Hiyoshi, Kohoku, Yokohama, Kanagawa 223-8522, Japan, 19911029@keio.jp
[3] Research Institute of Science for Safety and Sustainability, National Institute of Advanced Industrial Science and Technology, Central 5, 1-1-1 Higashi, Tsukuba, Ibaraki 305-8565, Japan, yuta.sugiyama@aist.go.jp
[4] Research Institute of Science for Safety and Sustainability, National Institute of Advanced Industrial Science and Technology, 16-1 Onogawa, Tsukuba, Ibaraki 305-8569, Japan, kubota.46@aist.go.jp
[5] Research Institute of Science for Safety and Sustainability, National Institute of Advanced Industrial Science and Technology, 16-1 Onogawa, Tsukuba, Ibaraki 305-8569, Japan, t.saburi@aist.go.jp
[6] Department of Mechanical Engineering, Keio University, 3-14-1 Hiyoshi, Kohoku, Yokohama, Kanagawa 223-8522, Japan, matsuo@mech.keio.ac.jp

ABSTRACT

We numerically investigated high-pressure hydrogen leakage from facilities in storage and transportation phases. In storage phase, assuming a tank placed in a hydrogen station, we examined unsteady diffusion distance up to 100 ms after leakage. A series of simulations led us to develop an equation of unsteady hydrogen diffusion distance as a function of mass flow rate, leakage opening diameter, and tank pressure. These results helped us develop a safety standard for unsteady hydrogen diffusion. In transportation phase, we simulated (in three dimensions) the dominant factor of steady mass flow rate from a square opening of a rectangular pipeline and the pressure distribution in the pipeline after leakage. The mass flow rate was smaller than the maximum mass flow rate and the pressure distribution converged to a steady state that was 16% higher than the pressure after the passage of expansion waves in a shock tube model. We introduced a theoretical model by dividing the flow with the leakage opening into two phases of the unsteady expansion waves' propagation and acceleration. The simulation results showed good agreement with the modeling equation when the shrink coefficient was set to 0.8. When the leakage opening was rectangular, the simulation results again showed good agreement with the modeling equation, suggesting that our simulated results are independent of the leakage opening shape.

1.0 INTRODUCTION

Current demands for hydrogen as a new energy source are rapidly expanding. Civilization has been consuming much fossil fuels. Burning of fossil fuels produces carbon dioxide and leads to global warming. In addition, fossil fuels are a finite resource. Researchers expect renewable energy, such as that from solar and wind, to replace fossil fuels; however, it needs to be stored in some form for stable use. One such alternative is the use of hydrogen produced by water electrolysis powered by renewable energy [1]. Hydrogen can also be produced by industrial processes and transported over long distances. In addition, hydrogen combustion products are completely nontoxic. Therefore, hydrogen-derived energy can conserve the environment and help establish a sustainable society. However, hydrogen has a high risk of explosion. The flammability of hydrogen–air mixtures ranges from 4 to 75 vol.%, which is much larger than that of hydrocarbon fuel–air mixtures. In addition, the minimum hydrogen ignition energy is approximately 0.02 mJ, which is much smaller than that of hydrocarbon fuel–air mixtures [2]. Therefore, acquiring parameters for safely storing and transporting hydrogen is of particular concern.

As the first step toward establishing a hydrogen society, household fuel cells and fuel cell vehicles are being spread in Japan. In 2015, 120,000 household fuel cells were sold. This is more than a 50 times increase compared to that in 2009, when fuel cell marketing began. Hydrogen stations are also being set up in Japan to supply hydrogen for fuel cell vehicles; there were 78 locations nationwide as of 2016. When hydrogen leaks from a hydrogen station and an ignition source come together to cause an explosion, it may result in serious damage to the surroundings [3]. It is therefore necessary to study hydrogen diffusion behavior in the context of leaks from high-pressure storage tanks in hydrogen stations. Many researchers have conducted theoretical, experimental, and numerical studies on hydrogen leakage explosions [4-7] and several experiments to show the relation between tank pressure and steady diffusion distance of hydrogen. Okabayashi et al. [6] conducted injection experiments and numerical analysis of high-pressure hydrogen gas in accordance with leakage opening diameter and total tank pressure. They investigated the relation between the time-averaged hydrogen concentration on the jet axis with respect to hydrogen diffusion and ignition behavior after leakage. Based on the time-averaged hydrogen concentration distribution upon injection of 82 MPa pressure from a 0.2-mm-diameter nozzle, the safety distance in a high-pressure hydrogen gas storage facility was defined as 8 m. Although many diffusion studies have been conducted in the context of safety distance, little is known about diffusion behavior in the unsteady state. The injection pressure is upward of 70 MPa, and it is dangerous to experimentally study the diffusion behavior. It is therefore useful to simulate the high-pressure hydrogen diffusion behavior in the atmosphere by using numerical analysis.

A transportation method is necessary for the use of hydrogen in a residential area. Currently, high-pressure gas and liquid hydrogen transportation is implemented. However, in the long term, hydrogen pipelines will be required for transporting large quantities of hydrogen from hydrogen stations to residential areas. In Japan, low-pressure hydrogen pipelines are only used in industry. In the hydrogen town at Fukuoka, a demonstration test was conducted in 2013, where a pipeline was introduced to supply hydrogen for residential use. In this pipeline, marker plates were laid underground to prevent construction accidents. Thus, safety measurements are essential for pipeline construction. In city gas pipelines, there are frequent plumbing and explosion accidents due to gas leakage from corrosion by long-term use. For example, in Japan, a road collapsed in Hakata station in November 2016 by approximately 15 m in depth due to water leakage during the subway extension work. This led to the breakage of underground water pipes and city gas pipeline, and filled the area with gas. Since the city gas supply was terminated, an explosion did not occur. Such hazardous situations may cause accidents and injury [8]. Since new pipelines are expensive, existing city gas pipeline facilities are to be used for hydrogen pipelines. However, there have been several city gas leakage accidents, and there may even be leakage from the hydrogen pipeline. Given that hydrogen has a higher risk of explosion than city gas, stricter safety measures are necessary. For this reason, considerable knowledge must be acquired prior to using hydrogen pipelines in residential areas.

Consequently, the risk of hydrogen leakage and diffusion from pipelines has been extensively studied, especially in recent years. Wilkening and Baraldi [9] investigated a scenario involving the release of 1.1 MPa pressure from a pipeline with a leakage opening. They investigated the effect of buildings and 10 m/s wind on combustion-range hydrogen concentration upon hydrogen or methane leakage into the ground. These conditions led to the choke state. It has been reported that if unburned gas accumulates around the structure, ignition readily occurs and the combustion speed increases regardless of the gas. However, since the sound speed of hydrogen is approximately 3 times that of methane, it leaks immediately. Therefore, compared to methane, hydrogen negligibly accumulates near a building regardless of wind. Okamoto et al. [10] conducted experiments and numerical calculations on the effects of specific gravity, pressure, and hydrogen concentration on leaks into the ground. The equilibrium of the penetration rate of hydrogen into the ground and the diffusion rate into the atmosphere became steady at 50 h after the initiation of leakage. Although much research focuses on hydrogen diffusion from the pipeline into the atmosphere and ground, few studies focus on the flow inside the pipeline after hydrogen leakage. For safety measures, the flow field of the pipeline is also important. In this context, it is necessary to deduce safety measures and standards for leakage. However, experiments with many parameters such as pipeline pressure, leakage opening area, and pipeline diameter cannot be performed

to a sufficient extent, due to high cost and risk. However, using numerical analysis, it is possible to investigate hydrogen behavior near the leakage opening, as well as to quantify the parameters such as pressure distribution and mass flow rate. Therefore, this paper aims to clarify the phenomena that occur after hydrogen leakage in the rectangular pipeline due to simplicity of the shape and to introduce modeling equations to obtain the mass flow rate and pressure after leakage using initial pressure and the leakage opening area.

2.0 Unsteady hydrogen diffusion distance from a high-pressure tank

Much research has focused on hydrogen diffusion distance in the steady state in order to determine the safety distance. However, there is less research on diffusion distance in the unsteady state. In this section, we investigate hydrogen diffusion distance in unsteady diffusion up to 100 ms after leakage.

2.1 Computational target and calculation conditions

The governing equations are two-dimensional axisymmetric compressible Navier–Stokes equations and chemical species conservation in terms of three chemical species: H_2, O_2, and N_2. The discretization method for the convective term is third-order SLAU [11-13], which is an AUSM family scheme, and the discretization method for the viscous term is second-order central difference. The time integration method is the two-stage Runge–Kutta method, and the turbulence model is the k - ω model, which is a two-equation model in RANS.

The computational target is the diffusion behavior in the atmosphere, resulting from injecting hydrogen, from a circular leakage opening of diameter D at pressure p_{jet}, which is greater than the critical pressure, and temperature T_{jet}. Figure 1 shows the grids used in the calculation and boundary conditions; the grids are shown in every 15 points and enlarged views of all points can be observed. In the coordinate system, the x-axis indicates the injection direction and the y-axis indicates the height. High-pressure hydrogen is injected from the boundary condition of the left-hand side. Since the physical quantity changes rapidly, the jet inlet point has a relatively high grid resolution. In the other locations, the grid size is stretched and a wide computational domain is taken. In all cases, 40 grid points are considered in each diameter of the leakage opening and the total grid points are approximately 140,000 (457 × 322).

We use the inflow condition for the leakage opening for the left-hand side of the boundary conditions and an adiabatic non-slip wall condition for the others. In addition, we use an axisymmetric condition for the lower end and zero-order extrapolation conditions as outflow conditions in the right-hand side and upper end. The total pressure and temperature of the ambient air are 0.101 MPa and 298 K, respectively. The jet pressure, temperature, and Mach number are given as the hydrogen jet conditions. The parameters include jet pressure, leakage opening diameter, and mass flow rate. We determine the mass flow rate based on the jet pressure and leakage opening diameter. Table 1 shows eight combinations of the jet physical quantities.

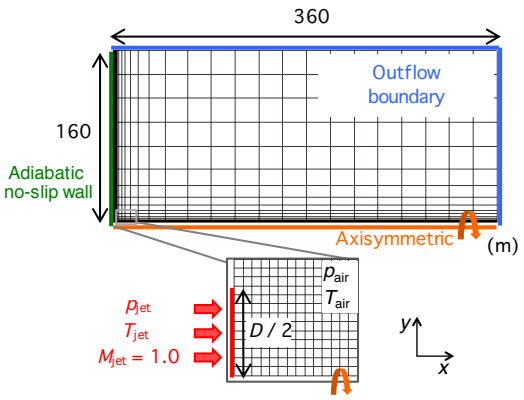

Figure 1. Calculation target ond conditions

Table 1. Each physical quantity for jet conditions

Case	Pressure [MPa]	Temperature [K]	Diameter [mm]	Mass flow rate [kg/s]
①	0.158	233	10	0.0122
②	1.30	233	10	0.100
③	10	233	10	0.795
④	20	233	10	1.59
⑤	40	233	10	3.18
⑥	40	233	20	12.7
⑦	10	233	100	77.1
⑧	40	233	100	309

The Mach number at the leakage opening is 1.0 because we consider the leakage opening to be choked from the ratio of the hydrogen jet pressure to atmospheric pressure. We inject high-pressure hydrogen from the circular leakage opening based on the choked condition that injection pressure, temperature, and injection mass flow rate are constant (because the decrease in tank pressure and mass flow rate can be considered negligible in the range of calculation times in this study). We assume the choked condition at the circular leakage opening, thereby obtaining the relations between p_0 and p_{jet} [Eq. (1)] and T_0 and T_{jet} [Eq. (2)].

$$\frac{p_{jet}}{p_0} = \left(\frac{2}{\gamma+1}\right)^{\frac{\gamma}{\gamma-1}} \tag{1}$$

$$\frac{T_{jet}}{T_0} = \frac{2}{\gamma+1} \tag{2}$$

where p_0 = tank pressure, Pa; p_{jet} = jet pressure at the leakage opening, Pa; T_0 = tank temperature, K; T_{jet} = jet temperature at the leakage opening, K; and γ = specific heat ratio.

2.2 Formula for classifying hydrogen unsteady diffusion distance

LaChance et al. [14] performed numerical analyses pertinent to high-pressure hydrogen diffusion in the steady state, and obtained a linear relation between the diffusion distance and mass flow rate on a double logarithmic chart. However, the hydrogen diffusion distance in the unsteady state is yet to be reported. We consider eight scenarios having different mass flow rates in the hydrogen diffusion calculation. Figure 2 shows the relation between the mass flow rate and hydrogen diffusion distance (t = 5, 20, 60, and 100 ms); the steady-state diffusion distance obtained from the numerical analysis by LaChance et al. [14] is also plotted.

In our numerical analysis, the diffusion distance is proportional to the mass flow rate at t = 60 and 100 ms, but not proportional at the initial injection stage (t = 5 ms). Therefore, we aim to deduce the hydrogen diffusion distances irrespective of time.

We first focus on five scenarios having a jet port diameter of 10 mm. At t = 5 ms, when the pressure and mass flow are large, the relation between the diffusion distance and mass flow rate is not proportional. To reflect a proportional relation, it is necessary to include the effect of difference in jet pressure and jet port diameter in the diffusion distance. Here, we introduce the normalized pressure p^* and diameter D^*.

$$p^* = \frac{p_{jet}}{p_{atmosphere}}, \quad D^* = \frac{D_{jet}}{D_{standard}} \tag{3}$$

where p^* is obtained by dividing the injection pressure p_{jet} by the atmospheric pressure $p_{atmosphere}$ and D^* by dividing the jet port diameter D_{jet} by the base diameter $D_{standard}$ (10 mm). The mass flow rate is proportional to the jet pressure and the square of the jet port diameter. Figure 3 shows the relation between the hydrogen diffusion distance X_{sim}, multiplied by the (1) square root of the normalized pressure and (2) normalized diameter, and the injection mass flow rate. From Fig. 3, $X_{sim} \times p^{*0.5} \times D^*$ and the mass flow rate $\dot{m}$ exhibit a proportional relation on a double-logarithmic chart [Eq. (4)].

$$X_{sim} \cdot p^{*0.5} \cdot D^* = C_1 \dot{m}^{C2} \tag{4}$$

The values of C_1 and C_2 are as follows.

$$C_1 = \left(X_{sim} \cdot p^{*0.5} \cdot D^*\right)_{\dot{m}=1}$$
$$C_2 = \frac{\log\left(X_{sim} \cdot p^{*0.5} \cdot D^*\right)_2 - \log\left(X_{sim} \cdot p^{*0.5} \cdot D^*\right)_1}{\log(\dot{m})_2 - \log(\dot{m})_1} \tag{5}$$

where C_1 is the value on the vertical axis when the mass flow rate $\dot{m}$ is equal to 1 kg/s and C_2 is the slope of the logarithmic value. In Eq. (5), the subscripts refer to any two points in the plot. We estimate

the values of C_1 and C_2 as a function of time. When an approximate curve of the exponential function of time is subtracted from the plot, C_1 and C_2 can be expressed as follows.

$$C_1 = 7.2767 \times t^{0.52237}$$
$$C_2 = 0.56638 \times t^{0.061729} \tag{6}$$

Therefore, using Eqs. (4) and (6), we calculate the hydrogen diffusion distance X_{model} as a function of time elapsed from the start of the injection, jet pressure, and leakage opening diameter. Equation (7) expresses the error from the simulation results as X_{sim}.

$$Error = 100 \times \frac{X_{model} - X_{sim}}{X_{sim}} \tag{7}$$

Figure 4 shows the relation between X_{sim} and X_{model}. Table 2 shows the average errors in each mass flow rate at each time point. We derive the average errors as the average of the absolute errors under each mass flow rate condition. The average error decreases with time, and the largest errors are at t = 5 ms (Table 2). Since the values are always overestimated at 5 ms in Fig. 4, we consider X_{model} to be valid in safety engineering for estimating the diffusion distance. Therefore, we use Eqs. (4) and (6) as the formulae for elucidating the hydrogen diffusion distance until t = 100 ms.

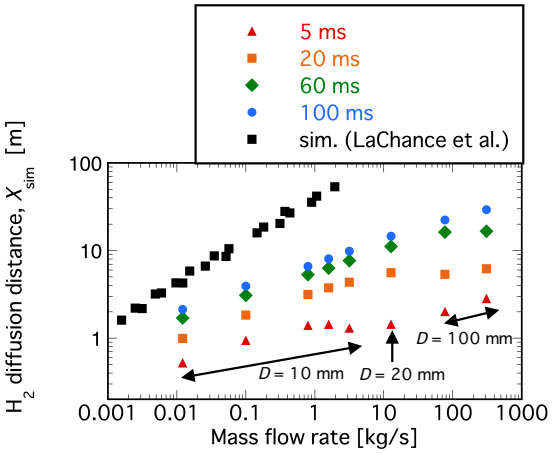

Figure 2. Relation between mass flow rate and diffusion distance

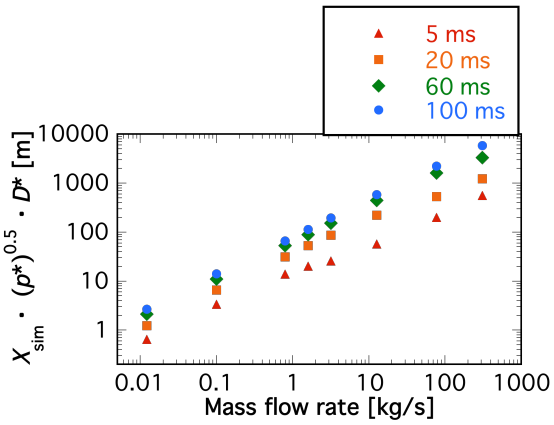

Figure 3. Relation between $X_{\mathrm{sim}} \times p^{*0.5} \times D^*$ and mass flow rate

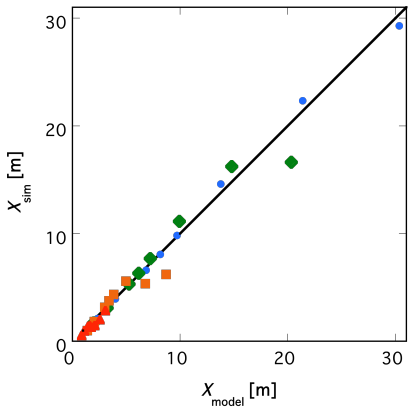

Figure 4. Relation between X_{sim} and X_{model}

Table 2. Average errors in each mass flow rate

Time [ms]	5	20	60	100
Average error [%]	27.1	19.2	8.92	3.76

3.0 Pressure field after leakage from a hydrogen pipeline

In this section, we report a three-dimensional analysis assuming hydrogen leakage from a square-shaped opening set at the top of a rectangular pipeline for investigating the mass flow rate and pressure distribution after leakage from the pipeline. From these results, we introduce modeling equations that express the steady mass flow rate and pressure after leakage at the middle of the pipeline.

3.1 Calculation conditions

The governing equations are three-dimensional compressible Euler equations or Navier–Stokes equations and an equation of chemical species conservation in terms of two chemical species: H_2 and air (N_2:O_2 = 3.76:1). The discretization method for the convection term is third-order SHUS [15], which is an AUSM family scheme. The time integration method is the two-step Runge–Kutta method. Gases are assumed to be calorically perfect.

The calculation target is a rectangular pipeline having a height h of 0.0925 m, depth of 0.0475 m, wall thickness of 0.00750 m, and length (between the edge of the leakage opening and the pipeline) of 3.00 m (Fig. 5). The leakage opening area A is 7.30 cm^2, 20.3 cm^2, or 56.3 cm^2. The right-hand side of Fig. 5 shows a leakage opening at the top of the pipeline, and one side of the leakage opening, D, is 2.70 cm, 4.50 cm, or 7.50 cm. We use the mirror boundary condition for both the left-hand and front sides of the pipelines, the adiabatic slip wall condition for the bottom and right-hand sides, and the zero-order extrapolation condition for the remaining sides. The pressure inside the pipeline $\boldsymbol{p_0}$ is 0.300, 0.500, or 1.00 MPa. The initial temperature in the pipeline is 293 K and the mole fraction of hydrogen is 1. The initial pressure and temperature of the ambient air are 0.101 MPa and 293 K, respectively, and the mole fraction of hydrogen is 0. All regions are assumed to be in the stagnation state. For the leakage opening, we place 75 × 75 grid points and 25 points for the wall thickness. Regarding the atmospheric condition, to reduce the computational cost, we stretch the grids and assume a wide area.

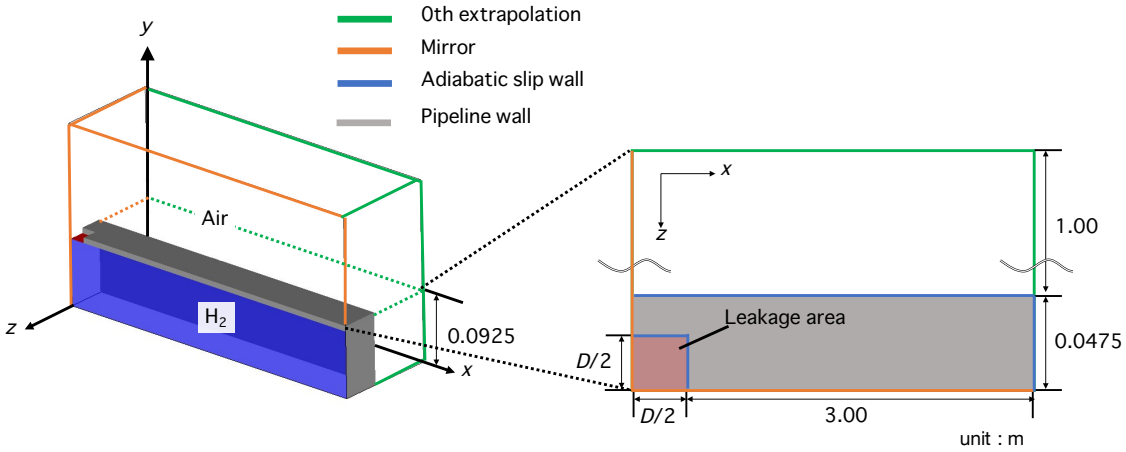

Figure 5. Calculation target (left: entire field, right: area at y = 0.0925 m)

3.2 Simulation results

In the pipeline with the leakage opening, the pressure gap induces air flow. From the simulation results, the mass flow rate history can be obtained. Figure 6 compares the simulation results using Euler and Navier–Stokes equations as governing equations. The results using Navier–Stokes equations are approximately 1% less than those using Euler equations (Fig. 6); consequently, the effect of viscosity is sufficiently small. Figure 7 compares the mass flow rate history as a function of leakage opening area when $p_0 = 0.3$ MPa. Figure 8 compares the mass flow rate history as a function of initial pressure when $A = 20.3$ cm^2. From Figs. 7 and 8, the mass flow rate converges to a constant value under any condition because the flow is choked around the leakage opening. The steady mass flow rate depends on both initial pressure and leakage. Then, Fig. 9 shows a comparison between the simulation results with maximum mass flow rate that are obtained from following equation.

$$m_{max} = \frac{A\sigma^* p_0}{\sqrt{RT_0}}, \quad \sigma^* = \sqrt{\gamma\left(\frac{2}{\gamma+1}\right)^{\frac{\gamma+1}{\gamma-1}}} \tag{8}$$

where $\dot{m}_{max}$ = maximum mass flow rate, kg/s; R = gas constant, J/(kg · K); T_0 = stagnation initial temperature in tank, K; p_0 = stagnation initial pressure in tank, Pa; A_e = leakage opening area, m^2; σ^* is a function of specific heat ratio; and γ = specific heat ratio.

The black line whose slope is 1 in Fig. 9 means that simulation results match with theoretical results from Eq. (8). From Fig. 9, simulation results do not match the maximum mass flow rate. Therefore, it is necessary to quantify these steady mass flow rates in a different way.

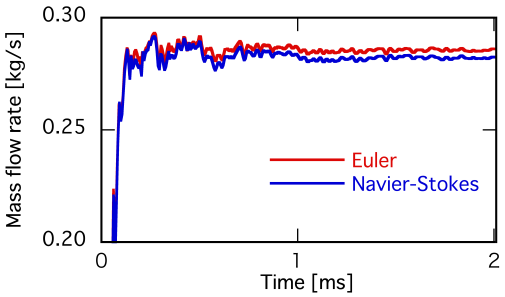

Figure 6. Effect of viscosity on mass flow rate history (p_0 = 0.3 MPa, A = 20.3 cm^2)

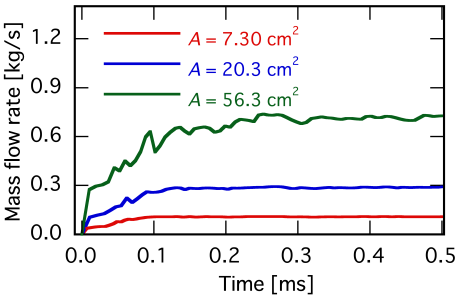

Figure 7. Mass flow rate history (p_0 = 0.3 MPa)

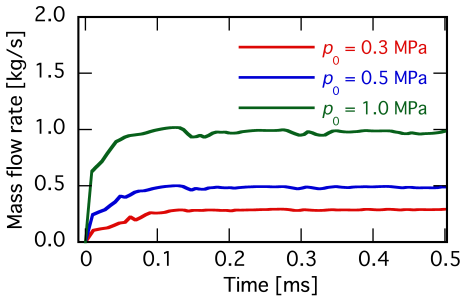

Figure 8. Mass flow rate history (A = 20.3 cm^2)

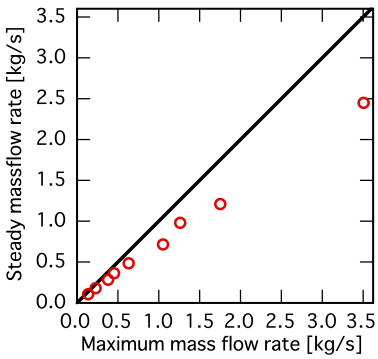

Figure 9. Comparison of mass flow rate with theory

Next, we investigate the pressure distribution. Figure 10 shows the history of pressure distribution at the middle of the pipeline in the x direction. The expansion waves propagate and the pressure inside the pipeline gradually converges, and pressure oscillations can be observed. The steady state of pressure in this distribution is p_1 (Fig. 10). The pressure decrease is only approximately 10%. The calculation target can be modelled as a one-dimensional shock tube model in Fig. 11. By using this model, the pressure after the passage of the expansion waves can be calculated by utilizing the initial pressure and specific heat ratio as follows.

$$\frac{p_H}{p_L} = \frac{2\gamma_L \mathrm{M}_s^{\,2} - (\gamma_L - 1)}{\gamma_L + 1}\left[1 - \frac{\gamma_H - 1}{\gamma_L + 1}\frac{a_L}{a_H}\left(\mathrm{M}_s - \frac{1}{\mathrm{M}_s}\right)\right]^{-\frac{2\gamma_H}{\gamma_H - 1}}$$

$$\frac{u_A}{a_L} = \frac{2}{\gamma_L + 1}\left(\mathrm{M}_s - \frac{1}{\mathrm{M}_s}\right), \quad \frac{p_H}{p_A} = \left(1 - \frac{\gamma_H - 1}{2}\frac{u_A}{a_L}\right)^{-\frac{2\gamma_H}{\gamma_H - 1}} \tag{9}$$

where subscript H = high pressure; subscript L = low pressure; subscript A = pressure after passage of expansion waves; M_s = Mach number of shock wave; a = sound speed, m/s.

Figure 12 shows comparison between the simulation results and shock tube model. The black line, whose slope is 1 in Fig. 12 means that the simulation results match the theoretical results from Eq. (9). From Fig. 12, values of p_1 at all conditions are higher than those of the shock tube model. Therefore, the flow in the pipeline with leakage opening cannot be simplified as the shock tube model, and a model that can calculate the steady pressure at the middle of the pipeline p_1 by using initial pressure and leakage opening area is required.

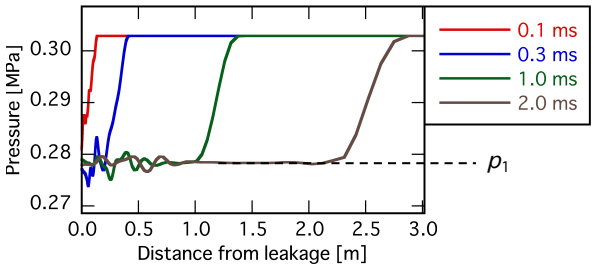

Figure 10. Pressure distribution history ($p_0 = 0.3$ MPa, $A = 20.3$ cm^2, $y = h/2$)

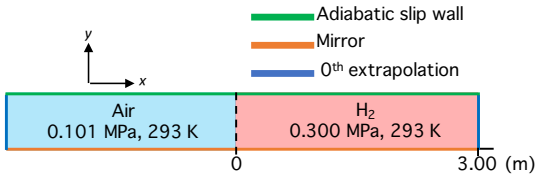

Figure 11. Calculation target of shock tube model

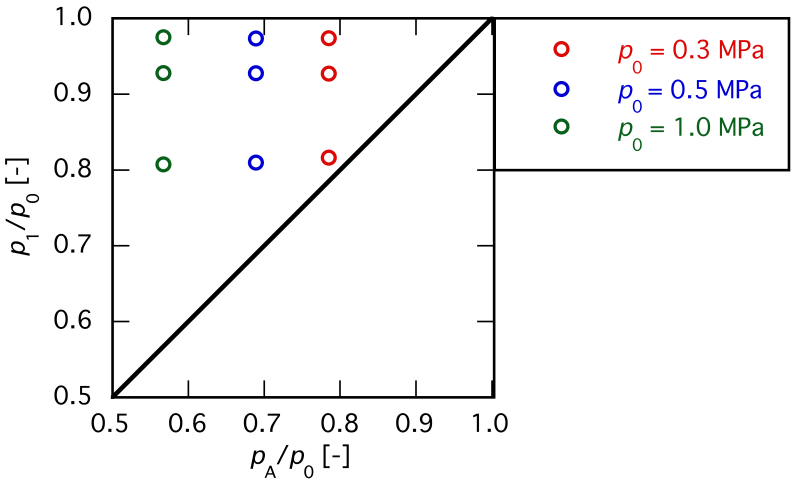

Figure 12. Comparison of pressure ratio with theory

3.3 Modeling equations

We explain our theory as follows. In our calculation target, the expansion waves propagate and area shrinkage after leakage accelerates the flow. Consequently, this flow can be described as being in two phases. The first phase is unsteady expansion waves' propagation and the second is flow acceleration as per area shrinkage. The purpose of our theory is to obtain the steady mass flow rate and pressure after passage of the expansion waves, based on the initial pressure and leakage opening area. Figure 13 shows a schematic of the unsteady expansion waves' propagation. Subscript 0 indicates the initial condition, 1 indicates passage of the expansion waves, and 01 indicates the stagnation condition of 1. After passage of the expansion waves, the physical quantities (pressure, temperature and density) change in an isentropic process. In unsteady expansion, the total pressure and temperature also change. Section 3.2 ignored this process. Using these relations, when the ratio of the pressure after the expansion waves to the initial pressure p_1/p_0 is given, the temperature after the passage of the expansion waves, T_1, can be obtained from the following equation.

$$\frac{p_1}{p_0} = \left(\frac{\rho_1}{\rho_0}\right)^{\gamma} = \left(\frac{T_1}{T_0}\right)^{\frac{\gamma}{\gamma-1}} \tag{10}$$

The Riemann invariant is constant after the passage of the expansion waves. The initial velocity u_0 is 0, and we obtain T_1 using Eq. (10). We next obtain u_1 using the following equation.

$$\frac{2a_0}{\gamma-1}+u_0=\frac{2a_1}{\gamma-1}+u_1 \tag{11}$$

In condition 1, the isentropic equation is available. From the following equation, the total pressure p_{01} and total temperature T_{01} after passage of the expansion waves can be obtained.

$$\frac{T_{01}}{T_0}=\left(1+\frac{\gamma-1}{2}\mathrm{M}_1^2\right)\left(1+\frac{\gamma-1}{2}\mathrm{M}_1\right)^{-2}=\left(\frac{p_{01}}{p_0}\right)^{\frac{\gamma-1}{\gamma}} \tag{12}$$

where M_1 = Mach number of the condition after passage of the expansion waves.

Considering the next phase, Fig. 14 (a) shows a schematic of the acceleration by leakage opening. In our calculation condition, since we use the mirror boundary condition at the front and left-hand side, we model the flow field in the quarter system. Therefore, the leakage opening area is $A/4$. In addition, as there is shrinkage flow by the leakage opening, the region above the opening is where the flow is choked. This region is termed the choked flow area. Term c is the shrink coefficient and subscript c denotes the condition of the choked flow area. We express the choked flow area as $Ac/4$. Then, to simplify this target, we introduce one-dimensional modeling [Fig.14 (b)]. The flow direction differs, but the shrink-modulated flow area behaves in the same manner as Fig.14 (a). Using this model, one can assume one-dimensional isentropic steady flow. As the Mach number at the choked flow area, M_c, is 1, we obtain M_1 after the first phase. Therefore, the ratio of the choked flow area and pipeline area S can be obtained using the following equation, when the shrink coefficient c is set as an appropriate value. In our calculation target, we fix S as 9.25 × 4.75 cm^2 as shown in Fig. 5.

$$\frac{cA/4}{S}=\mathrm{M}_1\left[\frac{\gamma+1}{(\gamma-1)\mathrm{M}_1^2+2}\right]^{\frac{\gamma+1}{2(\gamma-1)}} \tag{13}$$

Finally, we obtain the mass flow rate (equal to the maximum mass flow rate) by using the following equation.

$$m_c=\sqrt{\gamma\left(\frac{2}{\gamma+1}\right)^{\frac{\gamma+1}{\gamma-1}}}\cdot\frac{p_{01}cA}{\sqrt{RT_{01}}} \tag{14}$$

where m_c = maximum mass flow rate at choked flow area, kg/s.

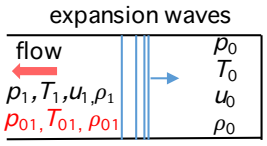

Figure 13. Schematic of unsteady expansion wave

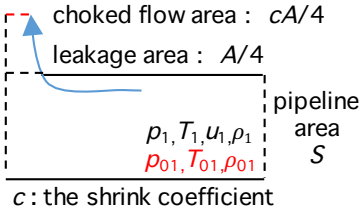

(a) flow in calculation

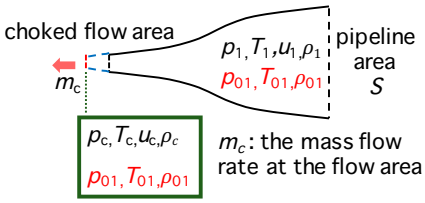

(b) one-dimensional isentropic steady model

Figure 14. Schematic of acceleration by the leakage opening

We obtain mass flow rate and leakage opening area from the pressure after passage of the expansion waves. Using this theory, the combination of the pressure ratio, mass flow rate, and leakage opening area can be decided. Figure 15 compares the steady mass flow rate between the simulations and theoretical results when p_0 = 0.3 MPa. We set the shrink coefficient c as 0.5, 0.8, and 1.0. The simulation results are consistent with the modeling equations when c is set as 0.8 (Fig. 15). Figure 16

compares the ratio of pressure after the passage of the expansion waves to the initial pressure when p_0 = 0.3 MPa. The simulation results are consistent with the modeling equations when c is set to 0.8 (Fig. 16). We also calculate the maximum leakage opening area scenario. In other words, one side of the area is equal to the width of the pipeline. (A = 90.3 cm^2) Figure 17 compares the steady mass flow rate at each initial pressure and each leakage opening area when c is set to 0.8. Figure 18 compares the pressure ratio when c is set to 0.8 and p_0 = 0.3 MPa. As pressure ratio does not depend on initial pressure from both Fig. 12 and modeling equations, the results of pressure ratio in the p_0 = 0.3 MPa case are only shown. The black lines whose slopes are 1 in Figs. 17 and 18 mean that modeling results match with theoretical results. From Figs. 17 and 18, the simulation results of the steady mass flow rate and pressure ratio are found to be consistent with the modeling equation, when c = 0.8, in all conditions that comprise the maximum leakage opening case. Therefore, when the shape of the leakage opening area is a square, the modeling equation is applicable to any leakage opening area.

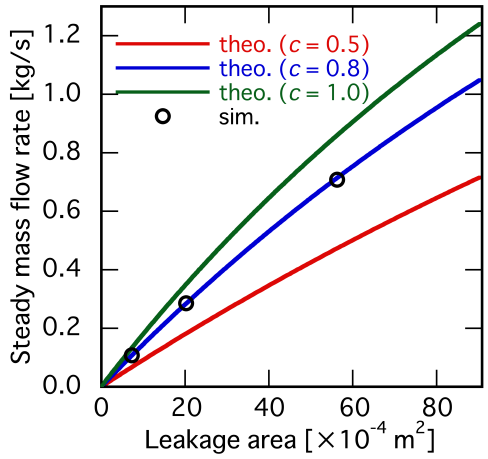

Figure 15. Comparison of steady mass flow rate (p_0 = 0.3 MPa)

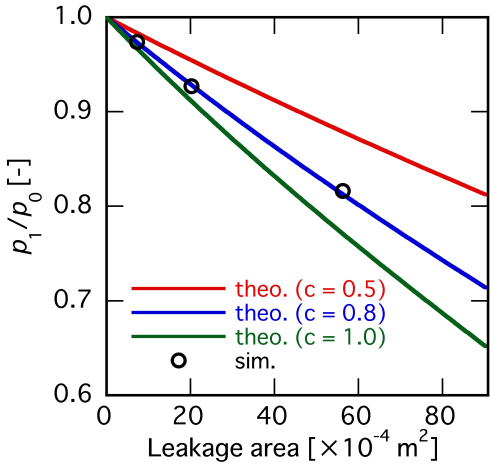

Figure 16. Comparison of pressure ratio (p_0 = 0.3 MPa)

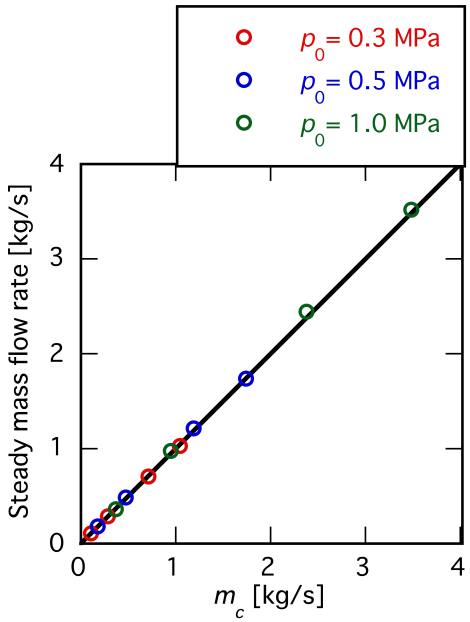

Figure 17. Comparison of steady mass flow rate with modeling results under all conditions (c = 0.8)

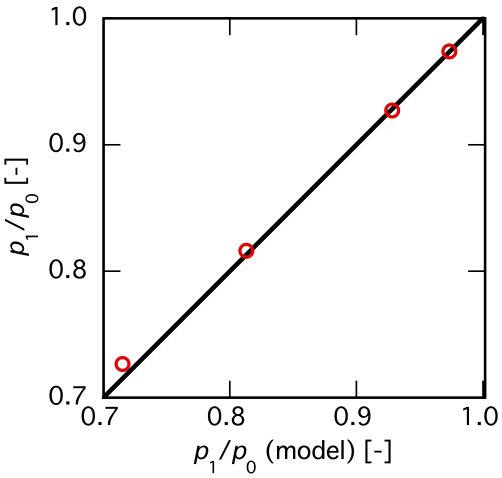

Figure 18. Comparison of pressure ratio with modeling results under all conditions (c = 0.8, p_0 = 0.3 MPa)

3.4 The effects of the shape of the leakage opening

So far, we have fixed the leakage opening to be a square. To elucidate the effect of the leakage opening shape, we apply a rectangular opening and compare the simulation results with the modeling equations. Figure 19 shows the new shapes of the leakage opening. Cases 1 and 2 have the same area, yet opposite aspect ratios. In case 3, the area is the same as per the previous calculation condition (20.3 cm^2), yet the aspect ratio is 4:1. We additionally set the initial pressure and c to be 0.3 MPa and 0.8, respectively. Figure 20 (a) compares the steady mass flow rate in all three cases. Since the areas used in cases 1 and 2 are the same, the mass flow rate is consistent. All scenarios are consistent with the modeling equation. Therefore, the simulation results of the mass flow rate (considering a rectangular leakage opening) are also consistent with the modeling equation when c = 0.8. Figure 20 (b) shows the comparison of the pressure ratio in all three cases. In case 1, the pressure ratio is negligibly different from the modeling results (0.2% error). All scenarios are almost consistent with the modeling equation. Therefore, the simulation results of the pressure ratio in the case of a rectangular leakage opening are also consistent with the modeling equation when c = 0.8.

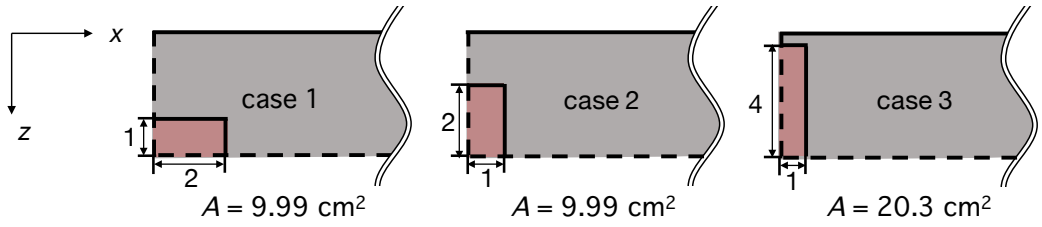

Figure 19. Calculation conditions of the rectangular opening (unit: aspect ratio)

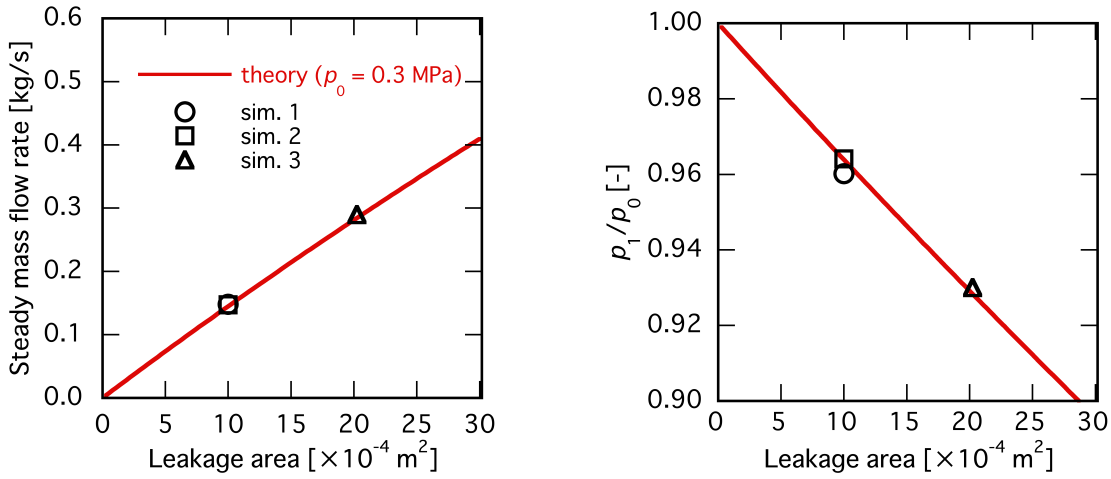

(a) steady mass flow rate (b) pressure ratio

Figure 20. Rectangular leakage opening scenario (c = 0.8)

4.0 Conclusions

In the context of storage, we construct an equation for the unsteady diffusion distance in a brief time interval (0–100 ms) from a high-pressure cylindrical hydrogen tank assuming a pressure of 0.2–40 MPa in a hydrogen station. The hydrogen diffusion distance can be obtained from the pressure in the tank, the leakage opening diameter, and the mass flow rate. In the context of transport, we investigate the mass flow rate and pressure field in a rectangular hydrogen pipeline, with a leakage defined as a square opening at the top. We perform an analysis using the initial pressure and leakage opening area as parameters. The mass flow rate converges at the steady state because the flow is choked at the leakage opening. In a pressure field inside the pipeline, the pressure converges at the steady state after passage of the expansion waves. By dividing the flow by a leakage opening into two phases of unsteady

expansion waves (propagation and acceleration), we theoretically obtain the steady mass flow rate and pressure after leakage. In the case of a pipeline consisting of the shape used in our analysis, the results show good agreement with the modeling equation when the shrink coefficient $c = 0.8$. When the leakage opening is rectangular, the simulation results also show good agreement with the modeling equation when $c = 0.8$, suggesting that our model is independent of the leakage opening shape.

REFERENCES

1. DOE Office of Energy Efficiency & Renewable Energy, Multi-Year Research, Development, and Demonstration Plan, https://energy.gov/eere/fuelcells/downloads/fuel-cell-technologies-office-multi-year-research-development-and-22, 2017,7,14
2. National Fire Protection Association, Recommended Practice on Static Electricity, NFPA 77, 2014
3. Ministry of Economy, Trade and Industry Commerce and Distribution Safety Group High Pressure Gas Safety Office, Technical standards of 82 MPa hydrogen stand draft, 2012 (Japanese)
4. The National Institute of Advanced Industrial Science and Technology, Hydrogen Network Construction Pipelines Safety Technology Survey Hydrogen Leakage Diffusion Behavior Survey Report, 2012 (Japanese)
5. Takeno, K., Okabayashi, K., Ichinose, T., Kouchi, A., Nonaka, T., Hashiguchi, K. and Chitose, K., On the Phenomena of Dispersion and Explosion of High-Pressurized Hydrogen Gas, Hydrogen Energy System, Vol. 30, No. 2, 2005, pp. 78-82
6. Okabayashi, K., Takeno, K., Hirashima, H., Chitose, K., Nonaka, T. and Hashiguchi, K., Introduction of Technology for Assessment on Hydrogen Safety, MHI Technical Report, Vol. 44, No. 1, 2007, pp. 17-19
7. Okabayashi, K., Takeno, K., Hirashima, H., Chitose, K., Nonaka, T. and Sakata, N., Leakage and Diffusion of High Pressure Hydrogen Gas, Safety Engineering, Vol. 44, No. 6, 2005, pp. 391-397
8. Sankei WEST, Hakata Station front collapse, http://www.sankei.com/west/news/161118/wst1611180058-n1.html, 2017,1,12
9. Wilkening, H. and Baraldi, D., CFD Modeling of Accidental Hydrogen Release from Pipelines, International Journal of Hydrogen Energy, Vol. 32, 2007, pp. 2206-2215
10. Okamoto, H., Gomi, Y. and Akagi, H., Movement Characteristics of Hydrogen Gas Within the Ground and Its Detection at Ground Surface, Journal of Civil Engineering and Science, Vol. 3, 2014, pp. 49-66
11. Kitamura, K. and Shima, E., Towards Shock-Stable and Accurate Hypersonic Heating Computations: A New Pressure Flux for AUSM-family Schemes, Journal of Computational Physics, Vol. 245, 2013, pp. 62-83
12. Kitamura, K. and Shima, E., A New Pressure Flux for AUSM-Family Schemes: Toward Shock-Stable, All-Speed Flux Functions for Hypersonic Heating, 24th Symposium of Computational Fluid Dynamics B12-3, 2010
13. Shima, E. and Kitamura, K., On New Simple Low Dissipation Scheme of AUSM-Family for All Speeds, AIAA Paper, 136, 2009
14. LaChance, J., Houf, W., Middleton, B. and Fluer, L., Analyses to Support Development of Risk-Informed Separation Distances for Hydrogen Codes and Standards, SANDIA REPORT, 2009
15. Shima, E. and Jounouchi, T., Role of CFD in Aeronautical Engineering (No.14) – AUSM Type Upwind Schemes, the 14th NAL Symposium on Aircraft Computational Aerodynamics, NAL SP-34, 1997, pp. 7-12